LAWRENCE
LIVERMORE
NATIONAL
LABORATORY

LLNL-PROC-407172

Modeling nonlinear Rayleigh-Tayor instabilities in fast z-pinches

A. R. Miles

September 23, 2008

2008 International Megagauss Conference
Novosibirsk, Russia
July 13, 2008 through July 18, 2008

Disclaimer

Modeling nonlinear Rayleigh-Taylor instabilities in fast z-pinches

Aaron R. Miles

Lawrence Livermore National Laboratory, Livermore, California 94550, (925)423-8131, miles15@llnl.gov

A simplified analytic model is presented to describe the implosion of a plasma column by an azimuthal magnetic field of sufficient magnitude to drive a strong shock wave into the plasma. This model is employed together with turbulent multimode Rayleigh-Taylor growth to investigate the mixing process in such fast z-pinches. These models give predictions that characterize limitations the instability can impose on the implosion in terms of maximum convergence ratios attainable for an axially coherent pinch. Both the implosion and instability models are validated with results from high-resolution numerical simulations.

I. INTRODUCTION

Rayleigh-Taylor (RT) instabilities [1,2] are ubiquitous in nature, and z-pinches offer an important platform for their study. A fast z-pinch is the implosion of a plasma cylinder behind a cylindrically convergent shock wave driven by a high-current discharge. In any such magnetic implosion, the total pressure and density gradients have opposite signs at the plasma-vacuum interface. Consequently, the interface is RT unstable. Instabilities can allow for local plasma compression beyond the radius at which hydro-magnetic equilibrium is established after first bounce, but also limit the maximum convergence ratio (CR) attainable for an axially coherent pinch.

In this paper, we employ a simplified analytic z-pinch model together with nonlinear multimode RT growth models based on the buoyancy-drag picture [3-6] to

investigate the mixing process in fast z-pinches. These models allow us to characterize limitations that the instability can impose on the implosion in terms of maximum *CR* for an axially coherent pinch. The instability model is compared and calibrated with 2D high-resolution numerical simulations.

II. IMPLOSION MODEL

We assume an infinitely long plasma column with initial radius R_0. An electrical current of arbitrary time-dependence is applied to the outer surface of the plasma column, resulting in a time-dependent implosion velocity $v(t) = dR(t)/dt$. If the time-dependent current is parameterized by $I(t) = I_0\beta(t)$, where I_0 is a characteristic dimensional current and the time-dependence is contained in the dimensionless function $\beta(t)$, then the magnetic pressure can be written as

$$P_B(t) = \frac{1}{2}\rho_0 u_0^2 \left(\frac{R_0}{R(t)}\right)^2 \beta^2(t), \tag{1}$$

where ρ_0 is the initial pre-shock plasma density and the characteristic speed u_0 is given by $u_0 \equiv I_0 / \left(R_0 c\sqrt{\pi\rho_0}\right)$ in cgs units. Within the fast z-pinch model, the only limitation on the driving current is that its magnitude is sufficiently high that a strong shock wave is driven into the plasma. The strong-shock limit allows for a very simple analytic model of the implosion based on three main statements: First, pressure balance between the shocked plasma and B-field. Second, equapartition of energy behind a strong shock relates the thermal and dynamic pressures. Finally, we need to identify a relationship between pressure, density, and velocity just behind the shock front with the same quantities at the

interface. If we neglect gradients in the shocked plasma and include a factor to account for cylindrical convergence, then the last two model components are expressed as

$$\frac{1}{\gamma-1}P_{th}^{*}=\frac{1}{2}\rho_{s}^{*}\frac{R_0}{R}v^2, \tag{2}$$

where v is the plasma-vacuum interface velocity and asterisks denote post-shock quantities.

We define dimensionless radius, velocity, and acceleration variables $\xi \equiv R/R_0$, $\tau \equiv t/t_0$, and $t_0 \equiv \frac{2}{3}\sqrt{\gamma+1}R_0/u_0$, in terms of which Eq. (2) becomes a first-order differential equation for the pinch radius:

$$\xi^{1/2}\frac{d\xi}{d\tau}=-\frac{2}{3}\beta(\tau). \tag{3}$$

Equation (3) can be analytically integrated (as long as $\beta(\tau)$ is analytically integrable) to give the dimensionless radius and acceleration:

$$\xi=\left[1-\int_0^{\tau}\beta(t)d\tau\right]^{2/3} \tag{4}$$

$$\frac{d\upsilon}{d\tau}=\upsilon\frac{d\upsilon}{d\xi}=\frac{4}{9}\frac{\beta[t(\xi)]}{\xi^{1/2}}\frac{d}{d\xi}\left(\frac{\beta[t(\xi)]}{\xi^{1/2}}\right)=-\frac{2}{9}\frac{\beta^2[t(\xi)]}{\xi^2}\left(1-2\xi\frac{d}{d\xi}\ln\left(\beta[t(\xi)]\right)\right) \tag{5}$$

Significantly, the dimensional drive current appears only in the characteristic time t_0. We apply the implosion model to two different functional forms for the drive current:

$$\beta(\mathrm{t})=\left(t/t_I\right)^n \tag{6a}$$

$$\beta(\mathrm{t})=\left(1-t/t_I\right)^n \tag{6b}$$

which we will refer to, respectively, as rising power law and falling power law.

Strictly speaking, the rising current forms validate our primary model assumptions (small plasma thermal pressure relative to magnetic pressure) for some

period of time. However, we anticipate reasonably accurate results as long as the model assumption is met on a timescale that is short compared to the pinch time, Similarly, the assumption of large magnetic pressure can potentially break down part way through the implosion in the decaying-current models, but starting with a sufficiently high current can in many cases ensure that this does not happen before the pinch time.

In the case of rising power-law current [Eq. (6a)], we find the plasma implodes according to

$$\xi = \left[1 - \frac{1}{n+1}\tau_I^{-n}\tau^{n+1}\right]^{2/3} = \left[1 - \frac{\tau_I}{n+1}\left(\frac{\tau}{\tau_I}\right)^{n+1}\right]^{2/3}. \tag{7}$$

The pinch time is defined by the time the radius is predicted to go to zero. For the power-law rising current, Eq. (7) gives

$$\tau_p = \left[(n+1)\tau_I^n\right]^{1/(n+1)} = \tau_I\left[(n+1)/\tau_I\right]^{1/(n+1)}. \tag{8}$$

The radius vs. time predicted by the model for a number of increments is plotted in Fig. (1a) for the cases of constant ($n = 0$) and linearly rising ($n = 1$) current. The characteristic current time t_I is chosen to the keep the implosion time constant and equal to the $n = 0$ value of $t_p = t_0$. That is, we choose $\tau_I = (n+1)^{-1/n}$.

With falling power-law currents [Eq. (6b)], the dimensionless radius is given by:

$$\xi = \left\{1 - \frac{1}{n+1}\tau_I\left[1 - \left(1 - \frac{\tau}{\tau_1}\right)^{n+1}\right]\right\}^{2/3} \tag{9}$$

Falling-current results are plotted in Fig. (1b). Choosing $n = 0$ of course gives the same constant-current result found in the rising-current form. Here again we have chosen the characteristic current times to give a fixed implosion time. The parameter choice of $n = 1/2$ together with $\tau_1 = 3/2$, which gives $\beta(t) = \sqrt{1 - 2\tau/3}$, is particularly significant in

that it gives constant implosion velocity. In this case post-shock $dv/dt = 0$ as the $1/R^2$ increase in magnetic pressure is exactly balanced by the decrease in drive current.

The implosion model is shown to compare well up to first bounce with 1D Ares [7] simulations for a variety of current profile forms, including constant current, linearly rising current, and the $\beta(t) = \sqrt{1 - 2\tau/3}$ falling current case predicted to give a constant implosion velocity [8]. The simulations use hydrogen gas described by tabular equation of state and conductivities, and we specify $P_B(I_0,R_0)/P_{th} \sim 10^4$ based on the dimensional current scale I_0, corresponding to a characteristic Mach number $M(I_0,R_0) \approx 90$.

III. INSTABILITY MODEL

An RT growth function can be used to characterize instability evolution due to time-dependent acceleration [9]. For the z-pinch implosion, we define the RT growth function

$$f(\tau) = \int_0^\tau d\tau \sqrt{-dv/d\tau - \gamma_D}\,, \tag{10}$$

where the first term under the square root is the contributions from interface acceleration in the lab frame, and the second is an effective gravity term present even for constant velocity implosion or hydro-magnetic equilibrium.

For the fast z-pinch, the interface acceleration term from the implosion model is given by Eq. (5). The effective gravity term due to the nonuniform B-field is

$$g_{eff} \equiv \frac{F}{m} = -\frac{P_B A}{\rho^* V^*} = -\frac{2}{R}\frac{P_B}{\rho^*} = -\frac{2}{R}\frac{P_{th}^*}{\rho^*}. \tag{11}$$

In our dimensionless units and assuming that density varies across the shocked plasma layer only due to cylindrical convergence, we have

$$\gamma_D \equiv g_{eff} t_0^2 / R_0 = -\frac{4(\gamma-1)}{9}\frac{\beta^2}{\xi^2} = -(\gamma-1)\frac{v^2}{\xi}. \qquad (12)$$

Inserting both terms into Eq. (10) for the growth function, we find

$$f(\xi) = \int_\xi^1 d\xi \sqrt{-\frac{1}{v}\frac{dv}{d\xi} - \frac{\gamma_D}{v^2}} = \sqrt{\gamma - \tfrac{1}{2}} \int_\xi^1 \frac{d\xi}{\sqrt{\xi}} \sqrt{1 - \frac{1}{\gamma - \tfrac{1}{2}} \xi \frac{d}{d\xi} \ln\left(\beta |t(\xi)|\right)} \qquad (13)$$

Based on self-similar growth [10] or bubble-merger [11,12] models that describe the inverse cascade from smaller to larger perturbation scales, multimode turbulent mix widths are given by [13,14]:

$$h_\alpha(t)/R_0 = \left[\sqrt{h_0/R_0} + \sqrt{\alpha} f(t)\right]^2 = h_{nl}/R_0 + \alpha f^2(t), \qquad (14)$$

where the parameter $\alpha_b \approx 0.06$ for bubbles in classical RT [15]. Such models can give asymptotic mix widths that are quadratic in f and independent of the initial conditions (perturbation amplitude and wavelength) once $\sqrt{\alpha} f(t) >> \sqrt{h_0/R_0}$. In order for this loss of memory of initial conditions to occur before the bubble tips reach the axis [$h_\alpha(t)/R = 1$], the model requires $\sqrt{h_0/R_0} << \sqrt{\xi_{min}}/2$, or $h_0/R_0 < \xi_{min}/400$. This result depends on the model parameter α only implicitly through the minimum radius ξ_{min}.

Turbulent mix widths predicted by the model for rising and falling power-law currents are shown in Fig. 2. The perturbations amplitudes are normalized to the instantaneous radius of the unperturbed interface, and are plotted against scaled radius. For reasons that will be discussed later, we use $\alpha = 0.108$ instead of the $\alpha \approx 0.06$ typical of classical RT. Constant current produces more mix than falling currents, and rising currents produce more mix than constant or falling currents.

We define the maximum convergence ratio for an axially-coherent pinch (CR_{max}) limited by instability growth as the CR based on the unperturbed interface position for

which instability bubbles are predicted to reach the origin. For varying n, the CR_{max} predicted by the asymptotic turbulent mix model is shown in Fig. 3. Again, we see that constant current produces more mix than falling currents, and rising currents produce more mix than constant or falling currents. For power-law rising currents at high n, CR_{max} asymptotes to a minimum value of about three.

For power-law falling currents the instability growth and even the nature of the implosion depend on the current decay time. In Fig. 4a, we show the pinch radius vs. time predicted by the model for a fixed $n = 1/2$ and four different values of τ_I. At infinite τ_I, the result is identical to the constant-current case. Below the critical scaled rise time $\tau_{I,crit} = 3/2$, the plasma does not fully implode. Consequently, for $\tau_I < \tau_{I,crit}$ we find that CR_{max} is limited by the 1D implosion rather than by the instability. At $\tau_{I,crit}$, CR_{max} is maximized, and above $\tau_{I,crit}$ it approaches the constant current value as expected.

IV. NUMERICAL SIMULATIONS

High-resolution 2D numerical simulations illustrate the nonlinear instability growth and facilitate calibration of the instability model. The numerical system is the same as that described earlier for the 1D calculations. In the 2D simulations, an initial perturbation is imposed on the outer surface of the plasma, with $ka = 0.45$, $\lambda_0/R_0 = 0.025$, and with 10 wavelengths in the domain. The initial mode in these calculations is only moderately resolved with $\lambda_0/\Delta z = 10$, where Δz is the axial grid resolution.

Density plots from simulations with three different current profiles are shown in Fig. 5 at various radii. Qualitatively, the results agree in several respects with the nonlinear instability models as applied to the fast z-pinch model. All three show

development of significant nonlinear growth initiated by the seed mode prior to first bounce. Constant current produces slightly more growth than the $n = 1/2$ falling-current case that gives constant implosion velocity in 1D. The linearly rising current produces much more growth than the constant- and falling-current cases. In all three cases, an inverse cascade to larger scales is evident within about $CR = 2$, justifying application of the multimode instability growth model.

The bubble amplitude growth observed in the simulations is compared with Eq. (14) in Fig. 6. With an $\alpha = 0.06$ typical of classical multimode RT, the model-predicted growth is somewhat less than in the simulations. In Fig. 6 we therefore increase α to a value of 0.108, or 1.8 times the typical classical value, in order to achieve the best overall agreement with the simulations. In its present form, the model suffers from two main limitations that should cause it to underpredict the bubble acceleration, and consequently the instability growth. First of all, instability growth produces trailing mass and therefore reduces the plasma density at the unperturbed interface position. Second, the model uses the magnetic pressure at the unperturbed interface position rather than at the bubble tip, which is at smaller radius. Consequently, it should be no surprise that for best fit to data the model requires α higher than the classical RT value.

V. CONCLUSIONS

The implosion dynamics of a high-field fast z-pinch are described effectively by a very simple strong shock model that can be solved analytically for a variety of current forms. The model is valid up to first bounce as long as the magnetic pressure remains large compared to the initial plasma pressure.

Growth function analysis provides predictions for nonlinear multimode RT growth and places limits on the maximum convergence possible for an axially coherent pinch. Rising currents are predicted to produce faster growth, as a function of radius, than are constant currents, and decaying currents yield less growth than constant currents. Simulations exhibit growth that agrees with the model predictions with a turbulent-mix growth parameter α that is nearly twice as high as the typical for classical RT.

VI. ACKNOWLEDGEMENTS

In preparing this manuscript, I was greatly benefited by discussions with and input from Jim Hammer, Omar Hurricane, and Mark Adams. This work was performed under the auspices of the U.S. Department of Energy by Lawrence Livermore National Laboratory under Contract DE-AC52-07NA27344.

VII. REFERENCES

[1] J. W. S. Rayleigh, *Scientific Papers* (Cambridge University Press, Cambridge, 1899).

[2] G. I. Taylor, Proc. R. Soc. London, Ser A **201**, 192 (1950).

[3] R. M. Davies and G. I. Taylor, Proc. R. Soc. London, Ser. A **200**, 375 (1950).

[4] J. C. V. Hansom, P. A. Rosen, T. J. Goldsack, *et al.*, Laser Part. Beams **8**, 51 (1990).

[5] G. Dimonte and M. Schneider, Phys. Rev. E **54**, 3740 (1996).

[6] D. Oron, L. Arazi, D. Kartoon, *et al.*, Phys. Plasmas **8**, 2883 (2001).

[7] G. Bazan, Proceedings from the 2nd International Workshop on Laboratory Astrophysics with Intense Lasers, UCRL-ID-131978, ed. B. A. Remington, 42 (Lawrence Livermore National Laboratory, Livermore, CA 1998).

[8] A. R. Miles, "Nonlinear Rayleigh-Taylor instabilities in fast z-pinches", submitted to Phys. Plasmas, (2008).

[9] A. R. Miles, Phys. Plasmas **11**, 5140 (2004).

[10] D. L. Youngs, Physica D **12**, 32 (1984).

[11] K. I. Sharp, Physica D **12**, 3 (1984).

[12] J. Glimm and X. L. Li, Phys. Fluids **31**, 2077 (1988).

[13] K. I. Read, Physica D **12**, 45 (1984).

[14] G. Dimonte and M. Schneider, Phys. Fluids **12**, 304 (2000).

[15] G. Dimonte, D. L. Youngs, A. Dimits, S. Weber, M. Marinak, *et al.*, Phys. Fluids **16**, 1668 (2004).

Figure captions

Fig. 1. Fast z-pinch implosion model predictions of radius vs. time for (a) power-law rising current and (b) power-law falling current radius.

Fig. 2. Turbulent mix model with $\alpha = 0.108$ applied to fast z-pinch with power-law currents.

Fig. 3. Turbulent mix model ($\alpha = 0.108$) maximum convergence ratio for axially coherent fast z-pinch with power-law currents.

Fig. 4. (a) Radius vs time for several different falling current decay times, all with $n = 1/2$. Below the critical decay time, the plasma fails to implode completely. With $n = 1/2$, the implosion velocity is constant at a critical decay time. (b) CR_{max} vs current decay time with $\alpha = 0.108$. Perturbation growth is minimized at the critical decay time.

Fig. 5. Density plots from ARES simulations. Within each panel, the left-most image is from a simulation driven with an $n = 1/2$ falling current at the critical current decay time, the middle image is constant current, and the right-most image is linearly rising current.

Fig. 6. Comparison of nonlinear multimode model and 2D numerical simulations for constant, linearly rising, and $n = 1/2$ falling current with the critical current decay time. Lines denote model results with $\alpha = 0.108$, and symbols represent simulation results.

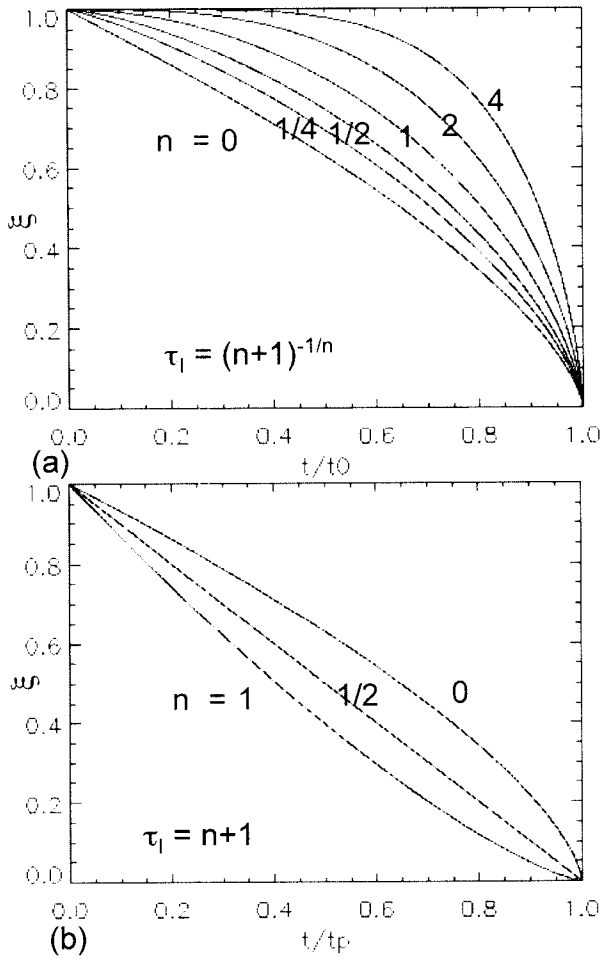
1.0
0.8
0.6
0.4
0.2
0.0
ξ
n = 0
1/4
1/2
1
2
4
τ_l = (n+1)^-1/n
0.0
0.2
0.4
0.6
0.8
1.0
t/t0
(a)
n = 1
1/2
0
τ_l = n+1
t/tp
(b)

Fig. 1

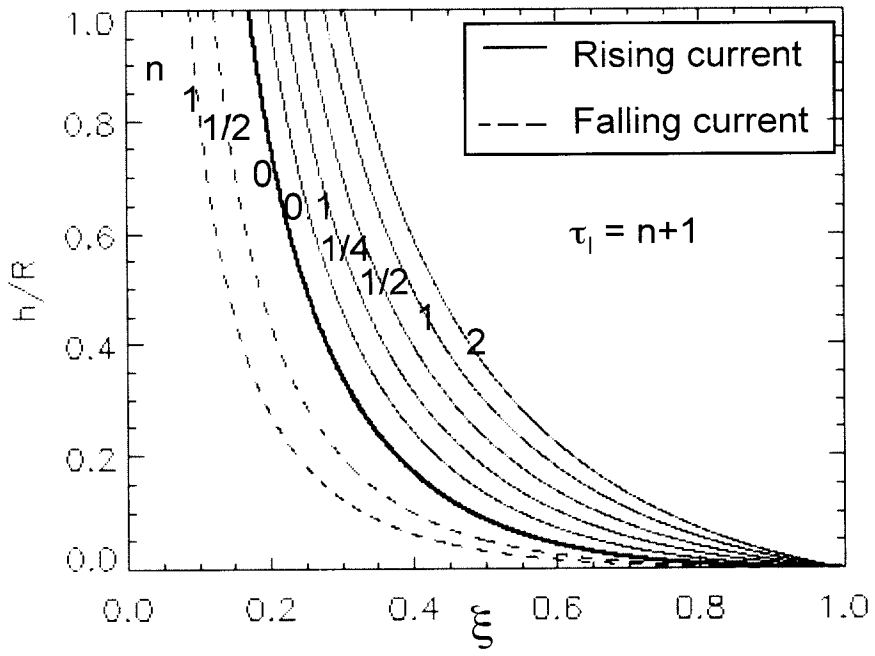
Rising current
Falling current
τ_I = n+1
n
1
1/2
0
0
1
1/4
1/2
1
2
h/R
ξ
0.0
0.2
0.4
0.6
0.8
1.0

Fig. 2

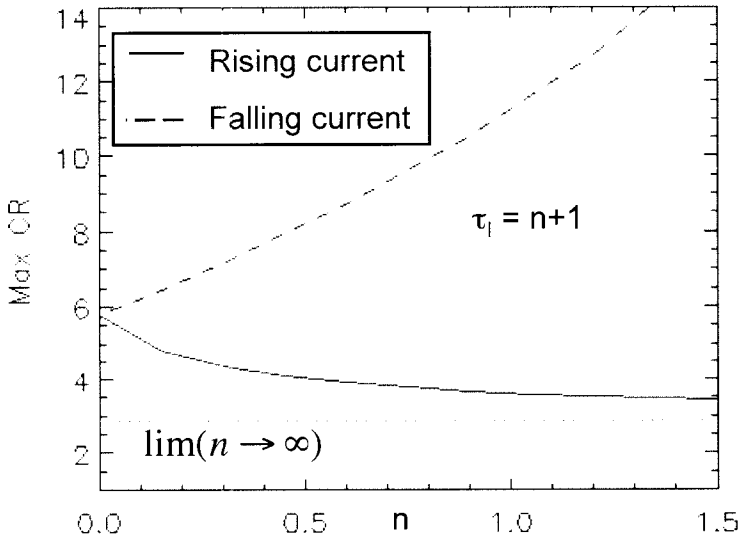
Rising current
Falling current
τ_l = n+1
$\lim(n \to \infty)$
Max CR
n
14
12
10
8
6
4
2
0.0
0.5
1.0
1.5

Fig. 3

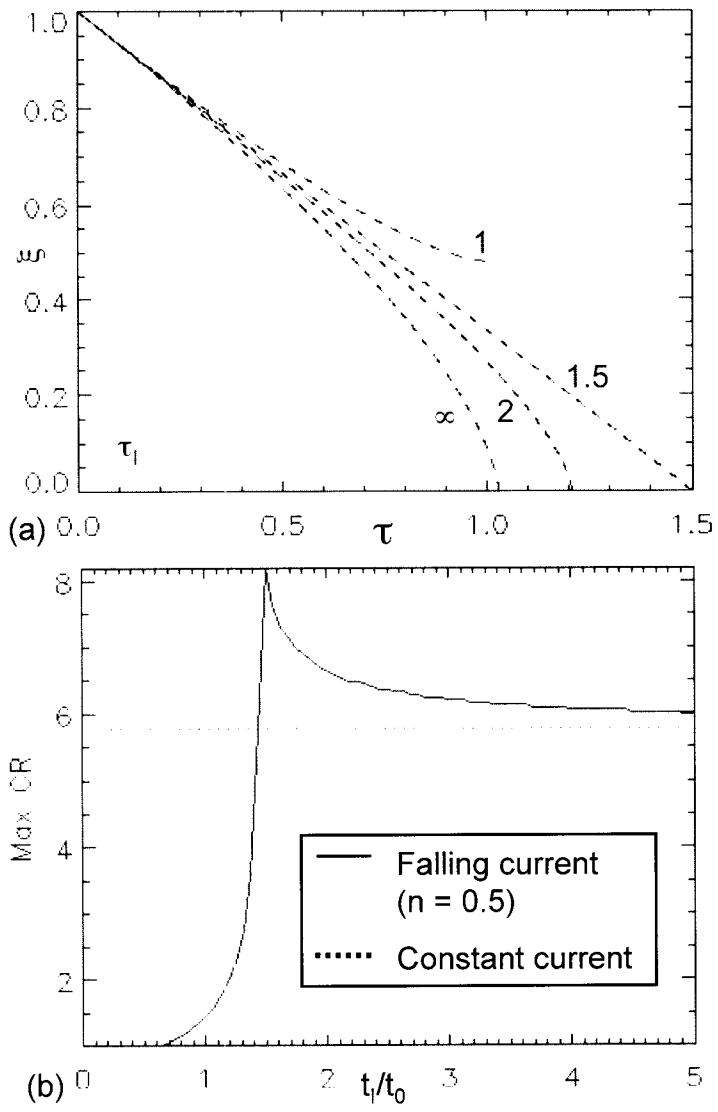
1.0
0.8
0.6
0.4
0.2
0.0
ξ
1
1.5
2
∞
τ_l
(a) 0.0
0.5
τ
1.0
1.5
8
6
4
2
Max CR
Falling current
(n = 0.5)
Constant current
(b) 0
1
2
t_l/t_0
3
4
5

Fig. 4

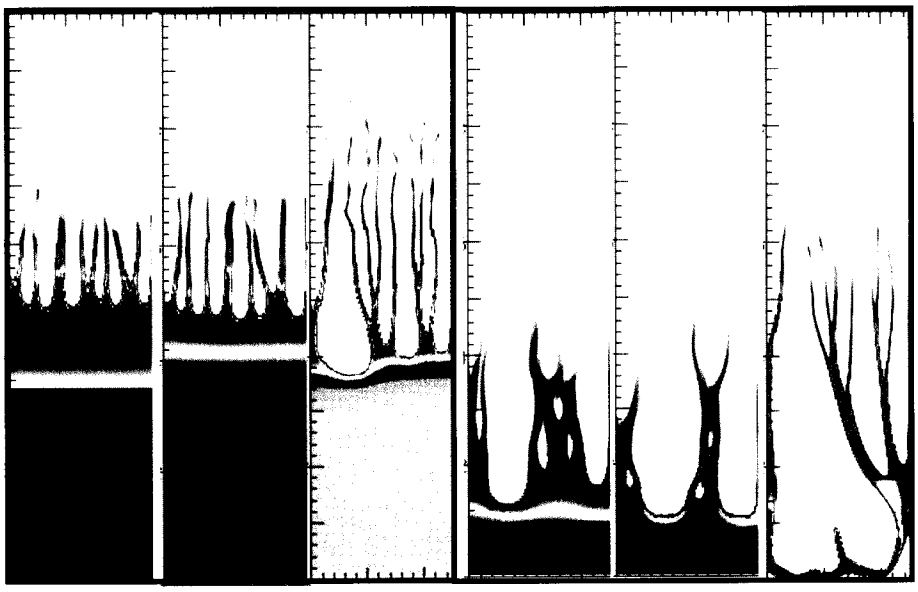

Fig. 5

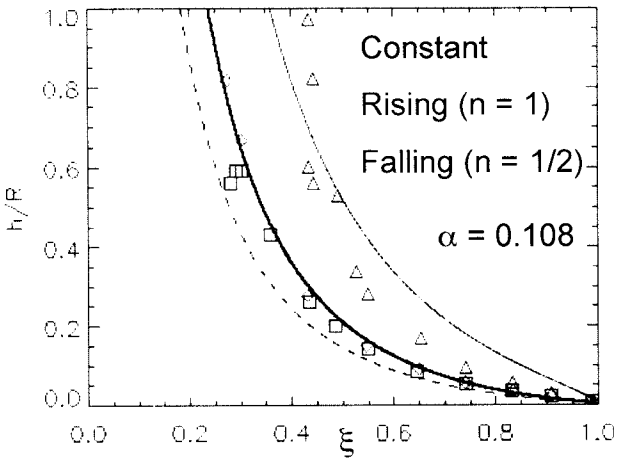

Fig. 6